Mamba based anisotropic diffusion model for speckle noise reduction in ultrasound images

Nhat Duy Pham[1], Marie Luong[1], Mounir Kaaniche[1], and Dinh Hoan Trinh[2]

[1] L2TI, Université Sorbonne Paris Nord, UR 3040, Villetaneuse, France
nhatduy.pham@edu.univ-paris13.fr
[2] Viettel AI, Hanoi, Vietnam

Abstract. Ultrasound imaging is widely used in clinical practice but is strongly affected by speckle noise, a signal-dependent pattern that blurs anatomical details and reduces diagnostic quality. Classical PDE-based despeckling methods provide interpretable solutions but rely on manually designed diffusion functions and parameter tuning, limiting adaptivity. In contrast, deep learning models achieve strong restoration performance but often lack interpretability and disregard the underlying PDE dynamics. In this paper, we propose a model-guided hybrid framework inspired by a recent hyperbolic–parabolic PDE scheme. Instead of analytically defining the diffusion function and solving an auxiliary equation, we approximate its key components using neural networks and learn the entire diffusion function in a data-driven manner. The diffusion evolution is reformulated as a learnable dynamical system, where a Mamba-based state space model, with high flexibility and efficiency in capturing complex and non-linear denoising dynamics, approximates the diffusion function and updates its components at each iteration. This allows the diffusion to adapt to local intensity and edge information while preserving the primary PDE structure. Extensive experiments on BUSI and AULI datasets show consistent improvements over classical diffusion methods and recent deep models in terms of PSNR, SSIM and PieAPP, effectively bridging model-based interpretability with data-driven flexibility for ultrasound despeckling. The source code is available at: https://github.com/duypham01/Mamba-Diff-US.

Keywords: Ultrasound imaging · Speckle reduction · Diffusion approximation · Neural networks.

1 Introduction

Ultrasound (US) imaging is widely used in clinical practice due to its safety, low cost, portability, and real-time capability. It plays a crucial role in the analysis of soft-tissue organs such as the thyroid, breast, and lungs [10,25]. Beyond routine diagnosis, US images are increasingly applied to automated analysis tasks, including segmentation [27] and image interpretation [21], which depend on reliable image quality. However, US images are often corrupted by noise, blur, and acquisition artifacts. Among these degradations, speckle noise remains one of the most fundamental and challenging characteristics of ultrasound imaging. Speckle is a granular, multiplicative, and signal-dependent artifact caused by the interference of echoes from sub-resolution scatterers [22]. While partially containing structural information, excessive speckle reduces contrast, masks fine details, and affects both visual interpretation and automated analysis. Therefore, dedicated speckle reduction methods are essential [3,19].

Classical US despeckling methods primarily build upon statistical modeling and variational diffusion frameworks. Early approaches include adaptive filters such as the Lee and Frost filters [7], which estimate local statistics to suppress speckle while preserving edges. Wavelet-based denoising techniques further improve noise reduction by separating signal and noise components in the transform domain [16]. In addition, Partial Differential Equation (PDE)-based models, such as Speckle Reducing Anisotropic Diffusion (SRAD) [26] and related nonlinear diffusion formulations [8], provide a physically interpretable framework by modeling despeckling as an edge-aware, gradient-driven diffusion process.

Deep learning has further advanced speckle suppression performance. US-Net [17] employs a parallel CNN design and adopts a residual learning strategy to better preserve anatomical boundaries. In contrast, LAD-CNN [18] introduces a lightweight attention-based autoencoder for detail retention and directly predicts the denoised image. HCTSpeckle [20] integrates Swin Transformer blocks to alleviate the quadratic computational cost of full-resolution self-attention by performing attention within shifted local windows, thereby improving efficiency while capturing contextual information. U-Tunnel-Net [5] further reveals that instance normalization is particularly suitable for addressing speckle noise in ultrasound images and modifies pooling strategies to enhance feature refinement.

Nevertheless, important limitations remain. While classical filtering and PDE-based methods offer strong interpretability and theoretical guarantees, they often require manual parameter tuning, and struggle in textured or low-contrast regions. In contrast, pure deep learning approaches achieve strong denoising performance but lack physical interpretability and theoretical grounding, potentially limiting robustness and clinical trust. To bridge this gap, recent works have explored hybrid and physics-informed frameworks that incorporate PDE principles or prior knowledge into neural networks, aiming to combine model-based reliability with data-driven flexibility [4,13,14].

Building on these observations, we propose a novel hybrid physics-informed framework for ultrasound speckle reduction that tightly integrates deep learning with a hyperbolic–parabolic PDE model of Majee *et al.* [12]. While prior works either approximate parabolic diffusion functions with UNet/ResUNet for natural [13] or ultrasound images [14], or use pretrained networks as priors to guide PDE-based despeckling in SAR images [4], our approach leverages the hyperbolic term to propagate fine structures and edges more effectively than purely parabolic schemes. Moreover, two Mamba-based networks are incorporated in our approximation model to learn distinct components of the diffusion function at each iteration, enabling globally informed, context-aware smoothing. The entire framework is trained end-to-end using paired noisy-clean images, effectively combining the stability, interpretability, and theoretical rigor of PDE-based modeling with the flexibility and ability of data-driven learning to capture complex patterns. Our main contributions can be summarized as follows:

- We propose a hybrid physics-informed framework that integrates a hyperbolic–parabolic PDE model with deep learning for ultrasound speckle reduction.
- We design a learnable parameter estimation strategy that adaptively estimates diffusion coefficients during the iterative PDE evolution.
- We validate the proposed approach on benchmark ultrasound datasets, demonstrating superior performance over recent deep learning baselines in terms of PSNR, SSIM, PieAPP, and subjective quality.

2 Methodology

2.1 Problem Formulation

In US denoising, speckle is commonly modeled as signal-dependent noise model [11]

$$I_0 = I + \sqrt{I}\,\mathcal{N}(0, \sigma^2), \tag{1}$$

which makes edge-preserving smoothing particularly challenging.

The problem of multiplicative noise removal is generally addressed through a denoising model based on total variation (TV) regularization, minimizing the energy function $E(I) = J(I) + \lambda H(I, I_0)$, where $J(I) = \int_\Omega \Phi(|\nabla I|)\, d\mathbf{x}$ is the TV term, Φ is a non-negative function controlling the penalization of image gradients, and $H(I, I_0)$ is the fidelity term. Here, $\Omega \subset \mathbb{R}^2$ denotes the spatial domain, ∇I is the image gradient, capturing local changes, and $|.|$ denotes the magnitude (Euclidean norm) of a vector. However, to avoid sensitivity to λ and insufficient denoising, most works typically set the fidelity term $H(I, I_0)$ to zero [28]. In this case, the minimum solution of the energy function E is given by

$$\frac{\partial E}{\partial I} = -\nabla \cdot \left(\Phi'(|\nabla I|) \frac{\nabla I}{|\nabla I|} \right).$$

Instead of solving $\frac{\partial E}{\partial I} = 0$ directly, most works adopt a gradient descent approach by introducing an artificial time variable t, resulting in the evolution equation $\frac{\partial I}{\partial t} = \nabla \cdot \left(\Phi'(|\nabla I|) \frac{\nabla I}{|\nabla I|} \right)$, which iteratively updates the image toward the minimum of the energy functional. Here, $I : \Omega_T := \Omega \times [0, T] \to \mathbb{R}$ denotes a speckled ultrasound image over the spatial domain Ω and a temporal interval $[0, T]$. Building on this idea, previous works on speckle noise reduction design a proper diffusion function $g(I) = \Phi'(|\nabla I|)/|\nabla I|$ to control the amount of smoothing while preserving edges.

For instance, SRAD [26] defines a diffusion function $g(I)$ based on the local image statistics to reduce speckle noise while preserving edges. However, this formulation is purely parabolic, which effectively smooths homogeneous regions but may oversmooth fine structures and is sensitive to manually tuned parameters. To overcome these limitations, hyperbolic PDE formulations introduce a second-order temporal term with damping, allowing wave-like propagation of image features [2]. In particular, Majee *et al.* [12] proposed a coupled hyperbolic–parabolic diffusion model, in which the hyperbolic equation governs the main diffusion process, while the parabolic equation serves as an auxiliary evolution equation to compute an edge-indicator variable that modulates the diffusion coefficient in the hyperbolic equation.

$$\frac{\partial^2 I}{\partial t^2} + \gamma \frac{\partial I}{\partial t} - \operatorname{div}\big(g(I,u)\nabla I\big) = 0, \qquad \text{in } \Omega_T, \tag{2}$$

$$\frac{\partial u}{\partial t} = h(|\nabla I_\xi|) - u + \frac{\nu^2}{2}\Delta u, \qquad \text{in } \Omega_T, \tag{3}$$

with boundary conditions $\frac{\partial I}{\partial n} = \frac{\partial u}{\partial n} = 0$ on $\partial\Omega_T$ and initial states $I(\mathbf{x},0) = I_0(\mathbf{x})$, $\frac{\partial I}{\partial t}(\mathbf{x},0) = 0$, and $u(\mathbf{x},0) = \big(G_\xi * |\nabla I_0|^2\big)(\mathbf{x})$ for $\mathbf{x} \in \Omega$. Here, G_ξ is a 2D Gaussian kernel with scale ξ, $I_\xi = G_\xi * I$, and $M_\xi^I = \sup_{\mathbf{x}\in\Omega} I_\xi(\mathbf{x})$. The diffusion control function $g(\cdot)$ is defined by the product of two terms as

$$g(I,u) = \frac{s^\alpha}{1+s^\alpha} \cdot \frac{1}{1+\imath|u_\xi|^\beta}, \quad s(\mathbf{x}) = \frac{\operatorname{abs}(I_\xi(\mathbf{x}))}{M_\xi^I} \in [0,1], \quad \mathbf{x} \in \Omega. \tag{4}$$

where $\alpha \geq 1$, $\beta \geq 1$, $\gamma > 0$, $\nu > 0$, and $\imath > 0$ are constants, $h : \mathbb{R}^+ \to \mathbb{R}^+$ is a bounded, Lipschitz continuous function. In (4), the first term acts as a *gray-level indicator* controlling intensity-dependent smoothing, while the second term as an *edge detector*, suppressing diffusion across edges, thereby enabling adaptive anisotropic diffusion.

2.2 Mamba-based Anisotropic Diffusion Approximation

The hyperbolic PDE model, described above, relies on different tuned hyperparameters to define the diffusion control function $g(\cdot)$. The choice of $g(\cdot)$ is crucial for determining diffusion behavior while suppressing noise, yet fixed formulations struggle when noise is signal-dependent or when image structures vary. To address these challenges, we replace the predefined diffusion function with a learnable approximation based on neural networks, and embed it within the discretized PDE solver, effectively combining the stability of model-driven approaches with the adaptability of data-driven learning.

To numerically approximate the continuous PDE, we discretize the time domain $[0,T]$ and denote by I^t the image at step t. Specifically, we learn the *gray-level indicator* and the *edge detector* via two Mamba-based neural networks, yielding $\mathcal{M}_1$ and $\mathcal{M}_2$ functions, respectively. To introduce a structured decomposition of the diffusion process, we reconstruct the diffusion function as the product of these two components, enabling a data-driven yet structured formulation of the diffusion dynamics:

$$\mathcal{M}_1(I^t) \approx \frac{s^\alpha}{1+s^\alpha}, \; \mathcal{M}_2(I^t) \approx \frac{1}{1+\imath|u_\xi|^\beta}, \; g(I^t) = \mathcal{M}_1(I^t)\cdot\mathcal{M}_2(I^t). \tag{5}$$

A key advantage of our approach is that it eliminates the need to manually tune the parameters α, $\imath$, and β, which are critical in traditional hyperbolic–parabolic PDE methods. Furthermore, our method removes the requirement to explicitly solve Eq. (3) for the auxiliary variable u, which is both computationally expensive and sensitive to noise. By learning both the gray-level indicator and edge detector directly from data, the diffusion function $g(I, u)$ becomes fully adaptive and data-driven, allowing the model to automatically adjust diffusion strength and edge sensitivity for each pixel. This not only simplifies implementation but also improves robustness and accuracy in speckle noise reduction, especially under varying imaging conditions.

Finite differences are used for both spatial and temporal approximations, while the weighted θ-scheme [9] is employed to discretize the nonlinear diffusion operator $L(I) := \mathrm{div}(g(I, u)\nabla I)$. Thus, Eq. (2) can be discretized as

$$\begin{aligned}(1 + 0.5\gamma\Delta t)I^{t+\Delta t} = 2I^t &+ (\Delta t)^2(1-\theta)L(I^t)\\ &+ (\Delta t)^2\theta L(I^{t-\Delta t}) + (0.5\gamma\Delta t - 1)I^{t-\Delta t}.\end{aligned} \tag{6}$$

Overall Network Flow. The proposed diffusion approximation model is summarized in Figure 1. Given an input noisy image I^0 (corresponding to $t = 0$), the image is iteratively updated according to Eq. (6). At each time step, I^t is fed into two Mamba networks to compute $\mathcal{M}_1(I^t)$, $\mathcal{M}_2(I^t)$, resulting in $g(I^t)$, which is then used to obtain $I^{t+\Delta t}$. This process is repeated for T iterations, producing the final output I^T. The Mamba architecture is described in Section 3.2. The overall network is trained by minimizing the mean squared error (MSE) between I^T and the ground-truth image I_{GT}: $\mathcal{L} = \|I^T - I_{GT}\|_2^2$.

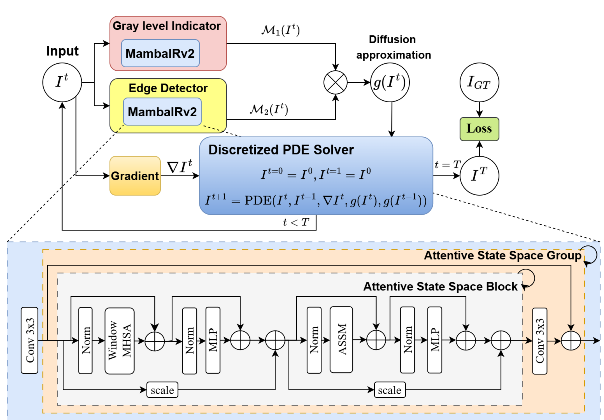

Fig. 1: The proposed Mamba-based anisotropic diffusion approximation model.

3 Experiments and results

3.1 Datasets

We evaluate our method on two publicly available US datasets: the Breast Ultrasound Dataset (BUSI) [1], which contains 788 2D ultrasound images, and the Annotated Ultrasound Liver Images (AULI) dataset [24], which consists of 560 2D images. All images were resized to 224×224. To simulate speckle degradation, multiplicative speckle noise was added according to Eq. (1) at three noise levels (15%, 30%, and 40%). For each dataset and noise level, the images were randomly split into training, validation, and testing sets with a ratio of 70%, 15%, and 15%, respectively. During training, paired data augmentation was applied, including random horizontal and vertical flipping as well as random rotation.

3.2 Implementation details

For the network architecture, we adopt MambaIRv2 [6] as the approximator of the diffusion control function g, using the `mambairv2_light` configuration. MambaIRv2 is a hierarchical vision backbone composed of Attention State Space Blocks (ASSBs), which integrate state-space modeling with local attention mechanisms. These blocks are organized into Attention State Space Groups (ASSGs) in a straight-through design. In our implementation, the architecture comprises three ASSGs, where the first uses two ASSBs and each of the remaining two includes one ASSB. The embedding dimension is set to 32 with a window size of 8. The upscale factor is fixed to 1 to preserve the input spatial resolution. For the diffusion process, we perform 40 iterations with a time step of $\Delta t = 0.25$, resulting in a total diffusion time of $T = 10$, while setting $\gamma = 1$, and $\theta = 0.4$. The learned diffusion maps are constrained to the range $[0, 1]$ to ensure stability and physical consistency. Parameter sharing is used across iterations for the two Mamba networks. The model was trained using the AdamW optimizer with an initial learning rate of 5×10^{-4}. A cosine annealing schedule was employed, with a minimum learning rate of 1×10^{-5}. Training was performed for 100 epochs with a batch size of 8.

3.3 Comparison methods and evaluation metrics

The proposed approach is compared with different state-of-the-art methods designed for ultrasound image despeckling, including U-Tunnel-Net [5], USNet [17], LAD-CNN [18], HCTSpeckle [20] and SRAD-ResUNet [14]. All competing methods are trained for 100 epochs with a batch size of 8. To ensure a fair comparison, each method is implemented following its original paper, including the reported loss functions, optimization strategies, and learning rate schedules. All methods are evaluated using traditional and perceptual image quality assessment metrics, including PSNR, SSIM [23] and PieAPP [15].

3.4 Results

Quantitative results: The performance of all methods on BUSI and AULI datasets at different noise levels is shown in Tables 1 and 2, respectively. Thus, among state-of-the-art methods, it can be observed that HCTSpeckle outperforms the other methods on the BUSI dataset, while SRAD-ResUNet and LAD-CNN yield better results on the AULI dataset. In contrast, our proposed approach achieves almost the best performance on both datasets and under different noise levels. For instance, compared to the second best method HCTSpeckle (resp. SRAD-ResUNet) on the BUSI (resp. AULI) dataset, the obtained average gain in terms of PSNR reaches 0.37 dB (resp. 0.59 dB).

Table 1: Objective evaluation on BUSI dataset at different noise levels. Best values are highlighted in **bold**, second-best ones are underlined.

Method	$\sigma = 0.15$			$\sigma = 0.3$			$\sigma = 0.4$		
	PSNR	SSIM	PieAPP	PSNR	SSIM	PieAPP	PSNR	SSIM	PieAPP
Input	21.53	0.503	1.74	15.93	0.241	1.72	13.92	0.179	1.88
U-Tunnel-Net [5]	27.76	0.827	<u>0.95</u>	26.98	0.770	<u>1.32</u>	25.16	0.688	<u>1.60</u>
USNet [17]	29.33	0.845	0.96	26.19	0.786	1.38	25.71	<u>0.700</u>	1.71
LAD-CNN [18]	28.76	0.772	1.78	27.82	0.740	1.96	25.84	0.657	2.26
HCTSpeckle [20]	<u>29.88</u>	**0.849**	1.02	**28.81**	<u>0.791</u>	1.39	<u>25.92</u>	0.695	1.65
SRAD-ResUNet [14]	29.49	0.833	1.01	28.28	0.786	1.41	24.74	0.644	1.66
Ours	**30.25**	<u>0.848</u>	**0.94**	<u>28.56</u>	**0.797**	**1.22**	**26.06**	**0.702**	**1.56**

Table 2: Objective evaluation on AULI dataset at different noise levels. Best values are highlighted in **bold**, second-best ones are underlined.

Method	$\sigma = 0.15$			$\sigma = 0.3$			$\sigma = 0.4$		
	PSNR	SSIM	PieAPP	PSNR	SSIM	PieAPP	PSNR	SSIM	PieAPP
Input	26.23	0.758	0.92	20.71	0.648	1.31	18.68	0.614	1.65
U-Tunnel-Net [5]	28.59	0.851	**0.73**	26.34	0.854	1.63	23.70	0.802	1.62
USNet [17]	26.79	0.888	1.50	25.82	0.861	1.49	22.32	0.823	1.55
LAD-CNN [18]	34.32	0.909	1.30	32.68	0.886	1.49	**31.84**	<u>0.876</u>	1.68
HCTSpeckle [20]	30.15	0.912	1.21	32.01	0.833	1.29	31.25	**0.879**	<u>1.41</u>
SRAD-ResUNet [14]	<u>35.52</u>	<u>0.932</u>	0.80	<u>32.77</u>	<u>0.894</u>	<u>1.22</u>	30.86	0.856	1.495
Ours	**35.71**	**0.934**	<u>0.79</u>	**33.36**	**0.902**	**1.09**	<u>31.82</u>	**0.879**	**1.38**

Qualitative results: To visually assess the denoising quality, we present representative examples from BUSI and AULI datasets under different noise levels. Figure 2 shows the denoised images produced by the different methods, along with the noisy input and ground truth. Compared to existing methods, the proposed one better preserves fine structures and edges while effectively suppressing noise.

Sensitivity Analysis: The following experiments are conducted on the BUSI dataset with $\sigma = 0.3$.

• Mamba-based diffusion approximation: Two variants of our Mamba-based diffusion approximation are evaluated. The first consists in directly learning the

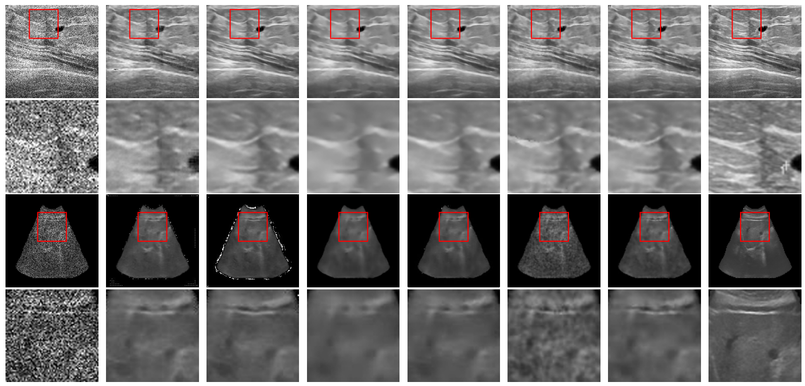

Fig. 2: Subjective comparison on two samples corrupted with speckle noise ($\sigma = 0.3$ for BUSI and $\sigma = 0.4$ for AULI). (a) Input, (b) U-Tunnel-Net, (c) USNet, (d) LAD-CNN, (e) HCTSpeckle, (f) SRAD-ResUNet, (g) Ours, (h) Ground Truth. Red rectangles indicate the zoomed-in regions for detailed comparison.

entire diffusion control function g, given by Eq. (4), using a single MambaIRv2 network. The second is the retained solution based on two separate MambaIRv2 models that approximate its two components $\mathcal{M}_1$ and $\mathcal{M}_2$ as defined in Eq. (5). As shown in Table 3, the proposed approach based on two networks outperforms the first variant using a single network.

Table 3: One vs two Mamba based diffusion approximation (40 steps, $\Delta t = 0.25$).

Approximation model	PSNR↑	SSIM↑	PieAPP↓
One Mamba	28.51	0.794	1.33
Two Mamba	**28.56**	**0.797**	**1.22**

• Impact of the diffusion steps: Table 4 shows the impact of the number of iterations on the performance of the proposed model. It can be seen that the model requires 40 steps for convergence.

Table 4: Impact of diffusion steps on the performance of the proposed model.

Steps	PSNR↑	SSIM↑	PieAPP↓
5	24.81	0.638	1.76
10	27.37	0.753	1.38
20	28.27	0.787	1.29
30	28.44	0.793	1.25
40	**28.56**	**0.797**	**1.22**
50	**28.56**	**0.797**	**1.22**

4 Conclusion

In this work, we propose a physics-guided hybrid framework for ultrasound speckle reduction by integrating a hyperbolic–parabolic PDE formulation with learnable diffusion parameter estimation. Rather than directly predicting the restored image, the model learns key diffusion parameters within the Majee scheme, enabling adaptive, spatially-aware evolution while preserving the structure and stability of PDE-based methods. Extensive experiments on BUSI and AULI demonstrate consistent improvements with respect to existing state-of-the-art methods. Future work will explore extension to other imaging modalities and evaluation on downstream tasks.

Acknowledgments. This research was partly supported by a French Government Scholarship managed by Campus France (No. 163978Z), and computational resources provided by the Jean Zay supercomputer, a French national HPC facility managed by GENCI (IDRIS) (No. AD011015859R1).

Disclosure of Interests. The authors have no competing interests to declare that are relevant to the content of this article.

References

1. Al-Dhabyani, W., Gomaa, M., Khaled, H., Fahmy, A.: Dataset of breast ultrasound images. Data in brief **28**, 104863 (2020) 6
2. Averbuch, A., Epstein, B., Rabin, N., Turkel, E.: Edge-enhancement postprocessing using artificial dissipation. IEEE Transactions on Image Processing **15**(6), 1486–1498 (2006) 4
3. Azzabou, N., Paragios, N.: Spatio-temporal speckle reduction in ultrasound sequences. In: Medical Image Computing and Computer-Assisted Intervention (MICCAI). pp. 951–958. Springer, Berlin, Heidelberg (2008) 2
4. Cheng, L., Xing, Y., Li, Y., Guo, Z.: A diffusion equation for improving the robustness of deep learning speckle removal model. Journal of Mathematical Imaging and Vision **66**(5), 801–821 (2024) 2
5. Gokmen, M., Arslan, B., Bumgardner, C., Imran, A.: An effective image despeckling and reconstruction approach using u-net based model and comparative analysis. Scientific Reports **15**(1), 33955 (2025) 2, 6, 7
6. Guo, H., Guo, Y., Zha, Y., Zhang, Y., Li, W., Dai, T., Xia, S.T., Li, Y.: Mambairv2: Attentive state space restoration. In: IEEE/CVF Conference on Computer Vision and Pattern Recognition (CVPR). pp. 28124–28133 (2025) 6
7. Gupta, N., Shukla, A., Agarwal, S.: Despeckling of medical ultrasound images: a technical review. International Journal of Information Engineering and Electronic Business **8**(3), 11 (2016) 2
8. Jain, S.K., Ray, R.K., Bhavsar, A.: A nonlinear coupled diffusion system for image despeckling and application to ultrasound images. Circuits, Systems, and Signal Processing **38**(4), 1654–1683 (2019) 2
9. Jovanović, B.S., Süli, E.: Analysis of finite difference schemes: for linear partial differential equations with generalized solutions, vol. 46. Springer Science & Business Media (2013) 5

10. Kremkau, F.: Diagnostic Ultrasound: Principles and Instruments. W.B. Saunders (2002) 1
11. Loupas, T., McDicken, W., Allan, P.L.: An adaptive weighted median filter for speckle suppression in medical ultrasonic images. IEEE Transactions on Circuits and Systems **36**(1), 129–135 (2002) 3
12. Majee, S., Ray, R.K., Majee, A.K.: A new non-linear hyperbolic-parabolic coupled pde model for image despeckling. IEEE Transactions on Image Processing **31**, 1963–1977 (2022) 2, 4
13. Ortega, J.V., Haas, M., Effland, A.: Learning diffusion functions for image restoration. In: IEEE International Symposium on Biomedical Imaging (ISBI). pp. 1–5 (2024) 2
14. Pham, N.D., Luong, M., Kaaniche, M., Trinh, D.H., Chetouani, A.: Ultrasound speckle denoising using resunet-based diffusion model. In: International Conference on Modelling, Computation and Optimization in Information Systems and Management Sciences. pp. 362–373. Springer (2025) 2, 6, 7
15. Prashnani, E., Cai, H., Mostofi, Y., Sen, P.: Pieapp: Perceptual image-error assessment through pairwise preference. In: IEEE/CVF Conference on Computer Vision and Pattern Recognition (CVPR). pp. 1808–1817 (2018) 6
16. Rakotomamonjy, A., Deforge, P., Marché, P.: Wavelet-based speckle noise reduction in ultrasound b-scan images. Ultrasonic Imaging **22**(2), 73–94 (2000) 2
17. Shen, Z., Tang, C., Xu, M., Lei, Z.: Removal of speckle noises from ultrasound images using parallel convolutional neural network. Circuits, Systems, and Signal Processing **42**(8), 5041–5064 (2023) 2, 6, 7
18. Shi, L., Di, W., Liu, J.: Ultrasound image denoising autoencoder model based on lightweight attention mechanism. Quantitative Imaging in Medicine and Surgery **14**(5), 3557 (2024) 2, 6, 7
19. Sivaanpu, A., Punithakumar, K., Zheng, R., Nguyen, K.C.T., Noga, M., Ta, D., Lou, E.H., Le, L.H.: Speckle noise reduction techniques in ultrasound imaging: A comprehensive review of the last two decades (2005–2024). Computer Methods and Programs in Biomedicine p. 109150 (2025) 2
20. Sivaanpu, A., Punithakumar, K., Zheng, R., Noga, M., Ta, D., Lou, E.H.M., Le, L.H.: Speckle noise reduction for medical ultrasound images using hybrid cnn-transformer network. IEEE Access **12**, 168607–168625 (2024) 2, 6, 7
21. Tmenova, O., Velikova, Y., Saleh, M., Navab, N.: Deep spectral methods for unsupervised ultrasound image interpretation. In: International Conference on Medical Image Computing and Computer-Assisted Intervention (MICCAI). pp. 200–210. Springer (2024) 1
22. Wagner, R.F., Smith, S.W., Sandrik, J.M., Lopez, H.: Statistics of speckle in ultrasound b-scans. IEEE Transactions on sonics and ultrasonics **30**(3), 156–163 (1983) 2
23. Wang, Z., Bovik, A.C., Sheikh, H.R., Simoncelli, E.P.: Image quality assessment: from error visibility to structural similarity. IEEE Transactions on Image Processing **13**(4), 600–612 (2004) 6
24. Yiming, X., Bowen, Z., Xiaohong, L., Tao, W., Jinxiu, J., Shijie, W., Yufan, L., Hongjun, Z., Tong, L., Ye, S., Rui, J., Guangyu, W., Jie, R., Ting, C.: Annotated ultrasound liver images (2022) 6
25. Yu, J., Duan, Y., Huang, Y., Wang, Y., Ling, R., Luo, W., Zhang, A., Xu, J., Ni, Q., Zhou, Y., et al.: Ultratwin: towards cardiac anatomical twin generation from multi-view 2d ultrasound. In: International Conference on Medical Image Computing and Computer-Assisted Intervention. pp. 608–617. Springer (2025) 1

26. Yu, Y., Acton, S.T.: Speckle reducing anisotropic diffusion. IEEE Transactions on Image Processing **11**(11), 1260–1270 (2002) 2, 3
27. Zhang, X., Chen, E.Z., Zhao, L., Chen, X., Liu, Y., Maihe, B., Duncan, J.S., Chen, T., Sun, S.: Adapting vision foundation models for real-time ultrasound image segmentation. In: International Conference on Medical Image Computing and Computer-Assisted Intervention (MICCAI). pp. 24–34. Springer (2025) 1
28. Zhou, Z., Guo, Z., Dong, G., Sun, J., Zhang, D., Wu, B.: A doubly degenerate diffusion model based on the gray level indicator for multiplicative noise removal. IEEE Transactions on Image Processing **24**(1), 249–260 (2014) 3